

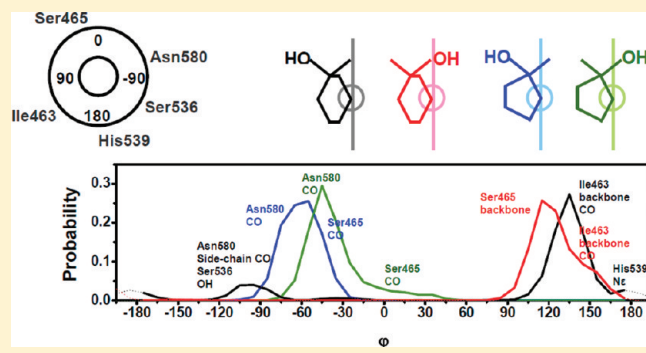
Investigation of the Differences in Activity between Hydroxycycloalkyl N1 Substituted Pyrazole Derivatives As Inhibitors of B-Raf Kinase by Using Docking, Molecular Dynamics, QM/MM, and Fragment-Based De Novo Design: Study of Binding Mode of Diastereomer Compounds

Julio Caballero,^{*†} Jans H. Alzate-Morales,[†] and Ariela Vergara-Jaque[†]

[†]Centro de Bioinformática y Simulación Molecular, Universidad de Talca, 2 Norte 685, Casilla 721, Talca, Chile

Supporting Information

ABSTRACT: N1 substituted pyrazole derivatives show diverse B-Raf kinase inhibitory activities when different hydroxy-substituted cycloalkyl groups are placed at this position. Docking, molecular dynamics (MD) simulations, and hybrid calculation methods (Quantum Mechanics/Molecular Mechanics (QM/MM)) were performed on the complexes, in order to explain these differences. Docking of the inhibitors showed the same orientation that X-ray crystal structure of the analogous (1*E*)-5-[1-(4-piperidinyl)-3-(4-pyridinyl)-1*H*-pyrazol-4-yl]-2,3-dihydro-1*H*-inden-1-one oxime. MD simulations of the most active diastereomer compounds containing *cis*- and *trans*-3-hydroxycyclohexyl substituents showed stable interactions with residue Ile463 at the entrance of the B-Raf active site. On the other hand, the less active diastereomer compounds containing *cis*- and *trans*-2-hydroxycyclopentyl substituents showed interactions with inner residues Asn580 and Ser465. We found that the differences in activity can be explained by considering the dynamic interactions between the inhibitors and their surrounding residues within the B-Raf binding site. We also explained the activity trend by using a testing scoring function derived from more reliable QM/MM calculations. In addition, we search for new inhibitors from a virtual screening carried out by fragment-based *de novo* design. We generated a set of approximately 200 virtual compounds, which interact with Ile463 and fulfill druglikeness properties according to Lipinski, Veber, and Ghose rules.



INTRODUCTION

RAF family kinases are major structures in the highly conserved mitogen-activated protein kinase (MAPK) signaling pathway (RAS–RAF–MEK–ERK) which relays signals from the extracellular media through receptor tyrosine kinases (RTKs) to the nucleus to promote the expression of genes involved in cell proliferation and survival.¹ Much attention has focused on this pathway as a prototypical signal transduction pathway that is aberrantly activated in many neoplasms. The Raf kinases are components of this pathway.² B-Raf is one of the Raf kinase isoforms, which most frequently mutated genes in human cancers.³ Many of the B-Raf mutations activate the kinase activity of B-Raf. Hence, B-Raf represents an excellent target for developing novel anticancer therapies. Indeed, several small molecules that inhibit B-Raf kinase have entered clinical development,^{4–6} and intensive effort has focused on novel inhibitor classes.⁷

The development of structural bioinformatics has profoundly benefited the drug discovery process. As part of an effort to find highly potent kinase inhibitors, computational models have had an essential contribution to the design of new molecules and the understanding of the relevant features for a good activity in the existing active molecules. Ligand-based drug design methods such

as quantitative structure–activity relationship^{8–14} and pharmacophore^{15,16} and receptor-based drug design methods such as docking,^{14,17,18} *de novo* design,^{19,20} QM/MM,^{13,17,21–23} and molecular dynamics (MD)^{24,25} have been used for studying kinase inhibitors. These methods have been scarcely applied for studying B-Raf kinase inhibitors.^{25–29}

In a recent report, Hansen et al. synthesized substituted pyrazoles, evaluated their IC₅₀ against B-Raf kinase, and tested them for cellular inhibition of the target pathway (IC₅₀ of ERK phosphorylation in melanoma cells: pERK).³⁰ They found that diastereomer compounds containing 3-hydroxycyclohexyl substituent are potent B-Raf inhibitors (compounds **1** and **2** in Figure 1); however, the replacement of this substituent by 2-hydroxycyclopentyl lead to lesser active diastereomer compounds (compounds **3** and **4** in Figure 1). In the current work, we studied the structure–activity relationships of the above-mentioned B-Raf inhibitors by using docking, MD simulations, and the QM/MM approach. First, the protein–ligand van der Waals complexes were obtained by means of molecular docking,

Received: July 4, 2011

Published: October 20, 2011

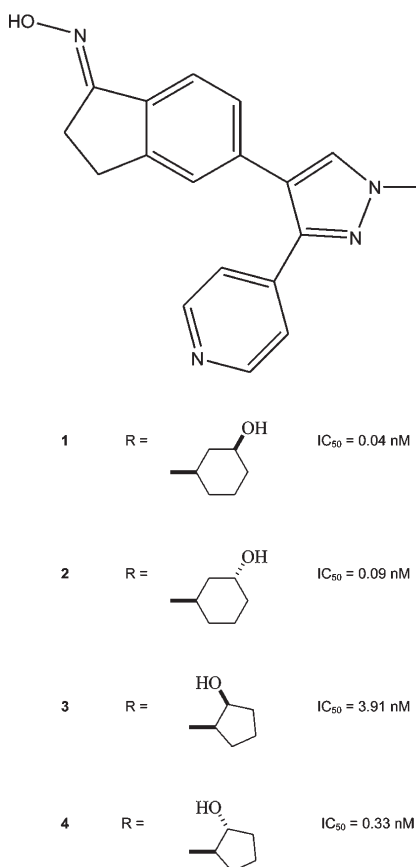


Figure 1. Pyrazole-based inhibitors and the biological activity effect of modification of the substituent at position 1 of the pyrazole scaffold. Atoms involved in the torsional angle φ are labeled.

then MD of the complexes were performed in order to describe the dynamics of the interactions between N1-substituents in the pyrazole ring and the residues at the entrance of the B-Raf pocket. Subsequently, a QM/MM derived scoring function was obtained for each compound using a set of frames from MD simulations. In addition, we proposed virtual candidates for future synthesis by using fragment-based *de novo* design.

METHODOLOGY AND COMPUTATIONAL DETAILS

Docking. In molecular docking, we attempt to predict the structure (or structures) of the intermolecular complex formed between two or more molecules. Docking has been widely used to suggest the binding modes of protein inhibitors.^{31–35} Most docking algorithms are able to generate a large number of possible structures, and so they also require a means to score each structure to identify those of most interest. In general, the “docking problem” is thus concerned with the generation and evaluation of plausible structures of intermolecular complexes.

Docking was performed by using ICM methodology.³⁶ The characteristics of ICM docking method have been described in previous reports.²⁵ The B-Raf kinase structure was used as a template for the docking simulations. The protein coordinates were extracted from the crystal structure of B-Raf kinase in complex with (1E)-5-[1-(4-piperidinyl)-3-(4-pyridinyl)-1H-pyrazol-4-yl]-2,3-dihydro-1H-inden-1-one oxime (accession code in Protein Data Bank: 3d4q). The structures of the inhibitors were

sketched by using Molecular Editor³⁷ of ICM software.³⁸ Protein and inhibitor structures were converted into ICM objects. During protein conversion process, hydrogens were added and they were optimized. Meanwhile, during ligand conversions, 2D representations were converted in 3D ones, partial charges were assigned, and rotatable bonds were identified. IcmPocketFinder³⁹ was used for identifying putative pockets with a tolerance value of 4.6. Initial ligand position and orientation, and box position and size, were kept according to the values suggested by the program. The maximum van der Waals repulsion was set to 4.0 Å in each docking experiment. The ten better docking poses for each ligand were analyzed by examining their relative total energy scores. The best docked position was determined by comparing docking poses and considering the total energy value. Among several similar docking poses, the more energetically favorable conformation was selected.

MD Simulations. Molecular dynamics of compounds 1–4 inside the B-Raf active site were studied using the OPLS-AA force field in explicit solvent with the SPC water model (OPLS-AA/SPC),⁴⁰ within the Desmond^{41,42} package for MD simulations. The initial coordinates for the MD calculations were taken from the docking experiments. The SPC water molecules were then added (the dimensions of each orthorhombic water box were 63 Å × 69 Å × 79 Å approximately, which ensured the whole surfaces of the complexes to be covered), and the systems were neutralized by adding Cl[−] counterions to balance the net charges of the systems. After the construction of the solvent environment, each complex system was composed by about 34000 atoms. Before equilibration and long production MD simulations, the systems were minimized and pre-equilibrated using the default relaxation routine implemented in Desmond. For this, the program ran six steps composed of minimizations and short (12 and 24 ps) molecular dynamics simulations to relax the model system before performing the final long simulations. After that, a first 2 ns long equilibration MD simulation was performed on each complex system, and it was followed for a 5 ns long production MD simulation. The OPLS-2005⁴⁰ force field was used, along with module MacroModel⁴³ to provide and check the necessary force field parameters for the ligands. When MacroModel performs an energy calculation, the program checks the quality of each parameter in use. Use of low quality parameters, especially torsional ones, may result in inaccurate conformational energy differences and geometries. All, bond, angle, torsional, and impropers, checked parameters were listed as high and medium quality force field parameters for all ligand studied. During MD simulations, the equations of motion were integrated with a 2-fs time step in the NVT ensemble. The SHAKE algorithm was applied to all hydrogen atoms; the van der Waals cutoff was set to 9 Å. The temperature was maintained at 300 K, employing the Nosé-Hoover thermostat method with a relaxation time of 1 ps. Long-range electrostatic forces were taken into account by means of the particle-mesh Ewald (PME) approach. Data were collected every 1 ps during the MD runs. Visualization of protein–ligand complexes and MD trajectory analysis were carried out with the VMD software package.⁴⁴

QM/MM Scoring Function. Twenty frames (selected every 250 ps) from long production MD simulations on each protein–ligand complex were chosen to perform this study. Water solvent box (far from 5 Angstroms (Å) of ligands) and counterion atoms were deleted from the systems in order to save computational time.

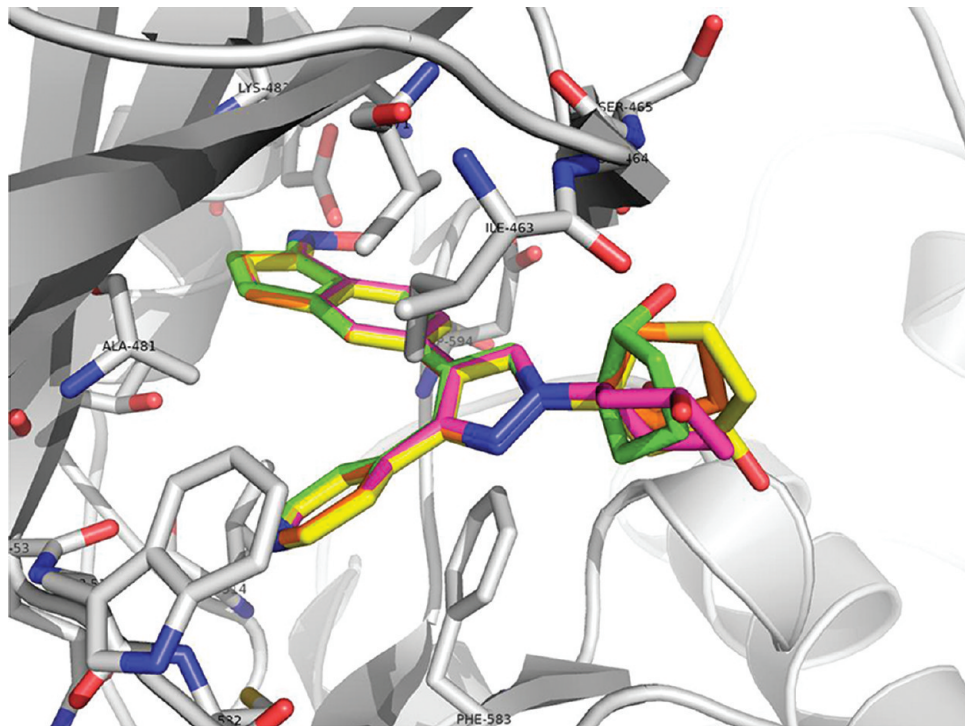


Figure 2. B-Raf/inhibitor complexes proposed by docking. Compounds 1–4 are represented in magenta, yellow, orange, and green, respectively. Hydrogens are omitted for clarity.

An energy minimization of every protein–ligand complex was performed, with Embrace application within module Macromodel from Schrödinger Suite, before to apply the QM/MM approach. To do this, the ligand and residues within 5 Å were selected as a first shell, which was allowed to move during energy minimization process. A second restricted shell (force constant of 200 kJ/mol Å² was applied) was selected including residues within 10 Å surrounding first shell. The remaining atoms beyond this distance were considered frozen during minimization. The PRCG (Polak–Ribiere Conjugate Gradient) method was used for energy minimization, with 15000 maximum steps of iteration and a convergence threshold criterion of 0.05 kJ/mol.

Subsequently, the QM/MM method was applied on each protein–ligand complex using the module Q-Site⁴⁵ from the Schrödinger Suite of computational programs. A single point energy calculation was performed on each system, both together and separated by several Angstroms of distance each other, where ligands were defined as part of the quantum mechanical (QM) region, and they were modeled at the density functional theory (DFT) level using the B3LYP/6-31G++** method and basis set, respectively. The protein and water molecules were defined as part of the molecular mechanics (MM) region, and they were modeled with the OPLS-2005 force field. QM/MM derived scoring function was obtained from arithmetical subtraction of energies of complexed and uncomplexed protein–ligand systems, according to eq 1

$$\Delta E_{QM/MM} = E_{complex} - E_{uncomplex} \quad (1)$$

Each ligand QM/MM energy was averaged over 20 conformations from MD frames.

Ligand-Fragment Based De Novo Design. We identified that most active compounds in ref 25 and the current work had HB interactions with the backbone carbonyl of Ile463. This

interaction was also identified by X-ray crystallography for potent N1 substituted pyrazole derivatives.³⁰ A combinatorial screening of R-groups containing a group that interacts with Ile463 attached to 1*H*-pyrazole ring was carried out to design new N1 substituted pyrazole derivatives. The RACHEL (Real-time Automated Combinatorial Heuristic Enhancement of Lead compounds) method was used.⁴⁶ RACHEL searches new substituents to create a derivative of a lead compound with optimal interactions with the active site of its receptor. The method requires defining an anchor bond to which components are attached. Potential complementary fragments were selected from a component database derived from the publicly available 3D structural database from the National Cancer Institute (NCI). During the RACHEL search, these components were attached to the anchor bond and were evaluated within the receptor cavity to optimize steric and electrostatic forces. The generalized scoring function derived from the VALIDATE training set⁴⁷ was used to select the best candidates. Druglikeness of the obtained compounds was evaluated, and the candidates were selected according to Lipinski,⁴⁸ Veber,⁴⁹ and Ghose⁵⁰ criteria.

■ RESULTS AND DISCUSSION

Compounds 1–4 were docked following ICM docking protocol. Comparison of the docking results shows that, in principle, all the compounds adopt the same binding mode identified by Hansen et al.³⁰ for compound (1*E*)-5-[1-(4-piperidinyl)-3-(4-pyridinyl)-1*H*-pyrazol-4-yl]-2,3-dihydro-1*H*-inden-1-one oxime (accession code in PDB: 3d4q) as shown in Figure 2. The similar binding mode is not surprising since all compounds contain the same scaffold and similar substituents. All compounds had the HB interactions with Glu501 and Cys532 and were surrounded by Val471, Lys483, Thr529, Leu514, Asp594, Phe583, Ala481,

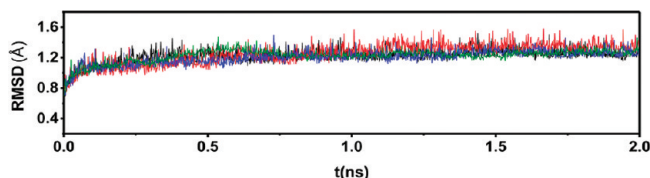


Figure 3. Time dependence of the rmsd for backbone from starting structures during the equilibration process. Rmsd for systems containing compounds **1–4** are represented in black, red, blue, and green respectively.

Table 1. Relevant Stable Distances between Atoms from the Inhibitors and Atoms from B-Raf during MD Simulations

compound	D1 (Å) ^a	D2 (Å) ^b
1	2.932 ± 0.125	3.476 ± 0.143
2	2.926 ± 0.126	3.462 ± 0.146
3	2.964 ± 0.135	3.483 ± 0.145
4	2.977 ± 0.143	3.466 ± 0.148

^a Distance between the nitrogen from the 4-pyridinyl group and the nitrogen from the backbone of Cys532. ^b Distance between the oxygen from the hydroxyimino group and the carboxylic carbon from the side-chain group of Glu501.

and Trp531 as described in previous literature for analogous compounds.²⁵ In addition, groups at position N1 of pyrazole scaffold (R substituents in Figure 1) were at the entrance of the pocket for all compounds. Since the only difference between compounds **1–4** is in this group, the interactions with the B-Raf residues involving these groups seem to be responsible for the differences between the inhibitory activities for them.

In a previous work, we studied the interactions established by N1 substituted pyrazole derivatives containing a 4-piperidinyl group (HB donor) and a tetrahydro-2H-pyran-4-yl group (HB acceptor) with the residues at the entrance of B-Raf active site and explained why the first one is a better inhibitor with respect to the second by considering the dynamics of the complexes.²⁵ Compounds **1–4** are similar to the above-mentioned compounds but contain hydroxy-substituted cycloalkyl groups at position N1 of the pyrazole scaffold, which can establish HB interactions as HB donors and acceptors at the same time. The most active compound **1** contains a *cis*-3-hydroxycyclohexyl group at position N1 of the pyrazole scaffold, while compound **2** contains a *trans*-3-hydroxycyclohexyl group at the same position; these compounds have similar activity and are potent B-Raf inhibitors. On the other hand, compound **3** contains a *cis*-2-hydroxycyclopentyl group at position N1 of the pyrazole scaffold, while compound **4** contains a *trans*-2-hydroxycyclopentyl group at the same position. Despite the small differences in the substituents, compounds **3** and **4** have considerable differences in their activities against B-Raf with respect to compounds **1** and **2** (Figure 1).

The dynamics of the interactions between the group at position N1 of the pyrazole ring and residues at the entrance of the B-Raf active site were studied for compounds **1–4** using MD simulations. The aim is to explain the differences in the activities for these compounds. The rmsds of the positions for all backbone atoms from their initial configuration as a function of simulation time (the first 2 ns of equilibration MD are represented) for all of the investigated systems are shown in Figure 3.

Table 2. Average Energies Obtained from QM/MM Single Point Calculations Applied to Snapshots of MD Simulations for Inhibitor–B-Raf Complexes

compound	IC ₅₀ (nM)	ΔG _{exp} (kcal/mol)	ΔE _{QM/MM} (kcal/mol)
1	0.04	−13.75	−101.55
2	0.09	−13.53	−100.53
3	3.91	−11.61	−95.95
4	0.33	−12.98	−98.93

The dependences of the rmsd values were tested to check whether convergence of the calculations was obtained and whether the equilibrated MD trajectory was stable. The rmsd values remain within 1.2 Å for all systems; this demonstrates the conformational stabilities of the protein structures. Along the simulations, the studied compounds were in the expected orientations.

In all simulations, the HB interactions between the inhibitors and residues Cys532 and Glu501 were established. Table 1 shows that these interactions were stable during all simulations. Distance between the nitrogen from the 4-pyridinyl group and the nitrogen from the backbone of Cys532 (D1 in Table 2) was around 2.9 ± 0.1 Å; while distance between the oxygen from the hydroxyimino group and the carboxylic carbon from side-chain group of Glu501 (D2 in Table 2) was around 3.4 ± 0.1 Å for all of the studied complexes. These specific interactions between B-Raf inhibitors and residues Cys532 (in the hinge region) and Glu501 (conserved glutamic acid) have been reported before by Wang et al.⁵¹ in the development of a series of pyrazolo[1,5-*α*]pyrimidine analogues. They were also stable during the MD simulation of analogous compounds.²⁵ Other important reported interactions within B-Raf active site include $\pi-\pi$ stacking interactions with residues Phe583 and Trp531 established by compound SB-590885, which is structurally similar to compounds studied here.⁵² These interactions were also established by compounds **1–4** during their MD simulations. We also verified the formation of water wire described in our previous study connecting N2 of pyrazole ring, Cys532, and Ser536 (sites WI, WII, and WIII in ref 25). To determine the presence of sites WI, WII, and WIII in the active site of complexes containing compounds **1–4** during the course of their MD simulation trajectories, volmap tool of VMD⁴⁴ was used. This tool allowed to generate the average occupancy of the water oxygens near the above-mentioned residues. The water occupancy plots for all the complexes are shown in Figure 4. These plots agree with the water wire formation for analogous complexes reported in ref 25. The distances between the oxygen of water molecules (at sites WI–WIII) and the N2 of the pyrazole ring, the backbone of Cys532, and the OH side-chain group of Ser536, respectively, for compounds **1–4** during their MD simulations were also analyzed (data not shown). As in previously studied inhibitors, we found that several water molecules participate in each HB, and water wires last the whole 5-ns simulation for all complexes.

We also analyzed the HBs formed between the groups at the position N1 of the pyrazole ring of the inhibitors and some residues at the entrance of B-Raf binding site. To trace the motion and the dynamics for these interactions and to determine whether the HBs were formed or broken, the interatomic distances describing them were monitored during the four developed MD simulations. Figure 5 shows the distances between the oxygen atom from the *cis*-3-hydroxycyclohexyl group of

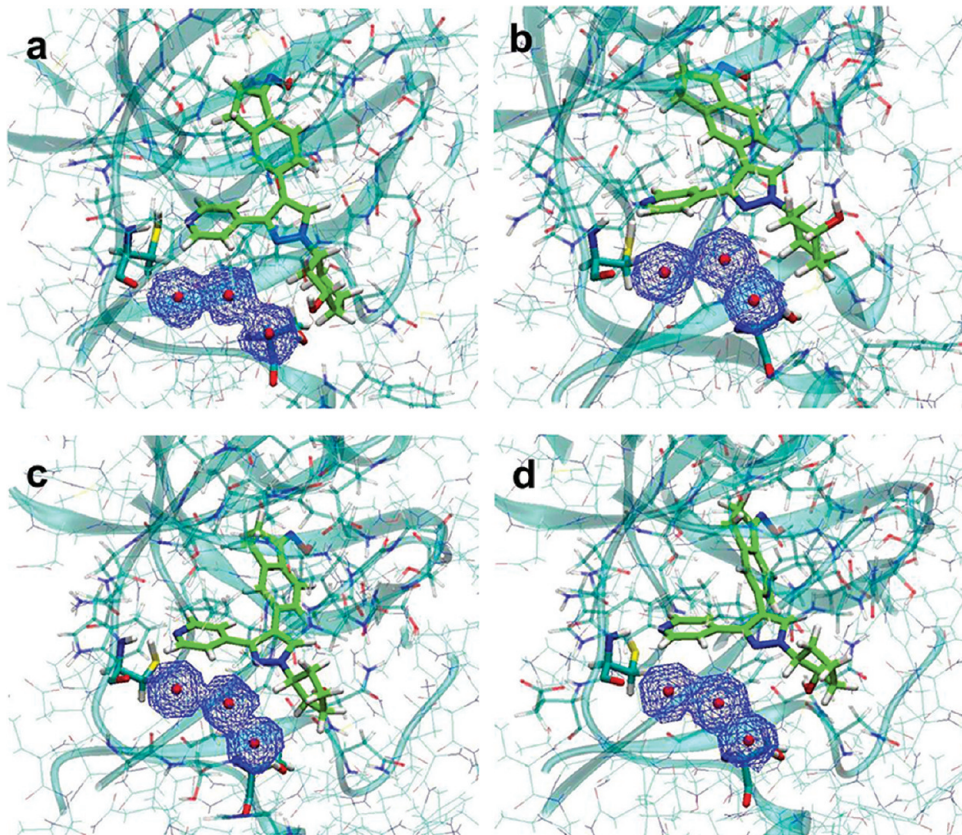


Figure 4. Occupancy data for water oxygens near residues Cys532 and Ser536 at the entrance of the active site of B-Raf for B-Raf/inhibitor complexes. Blue regions represent 50% occupancy.

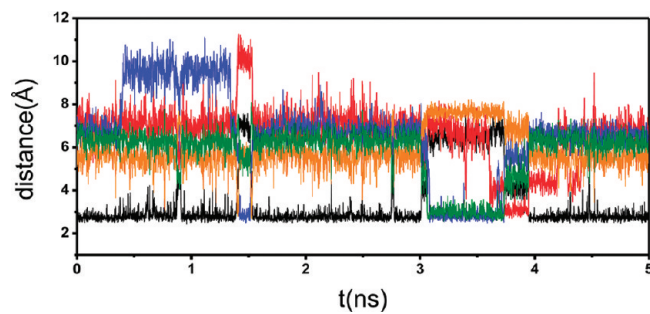


Figure 5. Distances between the oxygen atom from *cis*-3-hydroxycyclohexyl group of compound 1 (O1) and residues of B-Raf forming HB with this atom extracted from its 5 ns MD simulation. Distance between O1 and the backbone carbonyl group of residue Ile463 ($D_{O1-I463}$) is represented in black. Distance between O1 and the N ϵ side-chain atom of His539 ($D_{O1-H539}$) is represented in red. Distance between O1 and the carbonyl side-chain group of Asn580 ($D_{O1-N580}$) is represented in blue. Distance between O1 and the hydroxyl group of residue Ser536 ($D_{O1-S536}$) is represented in green. Distance between O1 and the backbone NH of residue Ser465 ($D_{O1-S465NH}$) is represented in orange.

compound 1 (O1) and residues of B-Raf forming HB with this atom during its MD simulation. The distance between the atom O1 and the backbone carbonyl group of residue Ile463 ($D_{O1-I463}$) took values around 2.8 ± 0.2 Å most of the time during all the 5-ns MD simulation, which means that an HB between the hydroxycyclohexyl from the inhibitor and Ile463 is established. $D_{O1-I463}$ takes higher values at certain intervals, when HB interaction between O1 and residue Ile463 was broken.

However, $D_{O1-I463}$ always returns to take values around 2.8 Å which indicates that compound 1 prefers to interact with Ile463 (Figure 6A). Atom O1 established other interactions when it did not interact with Ile463. The distance between the atom O1 and the carbonyl side-chain group of Asn580 ($D_{O1-N580}$) took values around 2.9 ± 0.4 Å from 1.4 to 1.5 ns and from 3.1 to 3.7 ns (Figure 5). In the second interval the distance between O1 and the hydroxyl group of residue Ser536 ($D_{O1-S536}$) also took values around 3.0 ± 0.2 Å. These values indicate that O1 established HB interactions with Asn580 and Ser536 at the same time during this period (Figure 6B). Finally, the distance between O1 and the N ϵ side-chain atom of His539 ($D_{O1-H539}$) took values around 3.1 ± 0.2 Å from 3.7 to 3.9 ns. During HB interaction with His539, O1 had additional HB interactions with a water molecule at position VIII of the water wire (see ref 25) and another water molecule located between O1 and the backbone carbonyl group of Ile463 (Figure 6C). The analysis of distances in Figure 5 indicates that O1 established the more stable HB interactions with Ile463 (Figure 6A) and can establish some temporal interactions with residues Asn580, Ser536, and His539 (Figure 6B and 6C).

Figure 7 shows the distances between the oxygen atom from *trans*-3-hydroxycyclohexyl group of compound 2 (O2) and residues of B-Raf forming HB with this atom during its MD simulation. Distance between the atom O2 and the backbone carbonyl group of residue Ile463 ($D_{O2-I463}$) took values around 2.8 ± 0.3 Å at certain intervals during the MD simulation, which means that an HB between the hydroxycyclohexyl from the inhibitor and Ile463 is established. During this interaction, O2

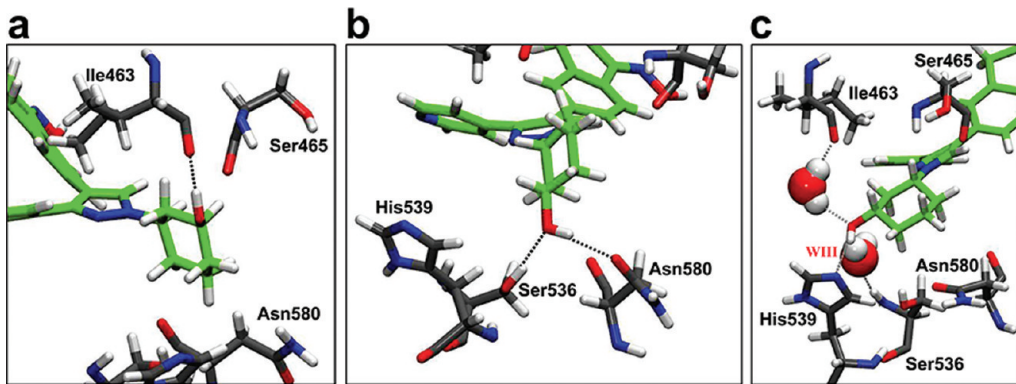


Figure 6. Hydrogen-bonding networks at the active site of the B-Raf-inhibitor complex from snapshots of the conformations obtained in 5-ns MD simulation for compound **1**: (A) when interactions with Ile463 are established, (B) when interactions with Asn580 and Ser536 are established, and (C) when interactions with His539 are established.

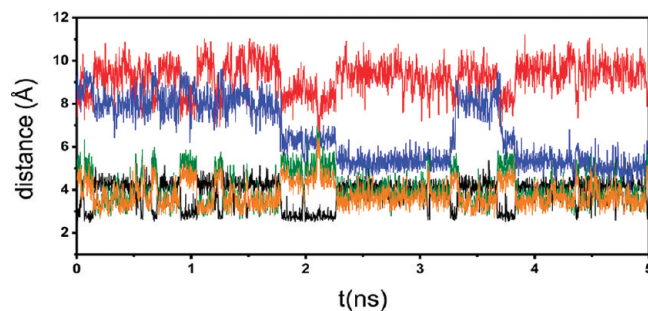


Figure 7. Distances between the oxygen atom from *trans*-3-hydroxycyclohexyl group of compound **2** (O_2) and residues of B-Raf forming HB with this atom extracted from its 5 ns MD simulation. Distance between O_2 and the backbone carbonyl group of residue Ile463 (D_{O_2-I463}) is represented in black. Distance between O_2 and the Nε side-chain atom of His539 (D_{O_2-H539}) is represented in red. Distance between O_2 and the carbonyl side-chain group of Asn580 (D_{O_2-N580}) is represented in blue. Distance between O_2 and the backbone carbonyl group of residue Ser465 ($D_{O_2-S465CO}$) is represented in green. Distance between O_2 and the backbone NH of residue Ser465 ($D_{O_2-S465NH}$) is represented in orange.

had an additional HB interaction with a water molecule forming a water bridge with the backbone NH of residue Ser465 (Figure 8A). $D_{O1-I463}$ frequently took higher values and returned to take values around 2.8 Å, which indicates that HB interaction between compound **2** and Ile463 (Figure 8A) is less stable compared to HB interaction established between compound **1** and the same residue. Distances between O_2 and the Nε side-chain atom of His539 (D_{O_2-H539}) and between O_2 and the carbonyl side-chain group of Asn580 (D_{O_2-N580}) took values higher than 4 Å during all the MD simulation, which indicates that compound **2** did not have HB interactions with residues His539 and Asn580. On the other hand, distances between O_2 and the backbone carbonyl group of residue Ser465 ($D_{O_2-S465CO}$) and between O_2 and the backbone NH of residue Ser465 ($D_{O_2-S465NH}$) took values close to 3 Å when D_{O_2-I463} takes higher values (Figure 7). This indicates that compound **2** established HB interactions with Ser465 when the HB interactions with Ile463 were broken (Figure 8B). Both compounds **1** and **2** established HB interactions with backbone carbonyl group of Ile463. This HB interaction was previously identified for the active analogous compound containing a 4-piperidinyl group in

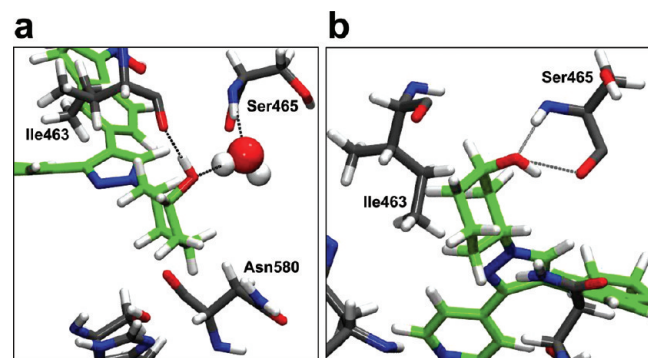


Figure 8. Hydrogen-bonding networks at the active site of the B-Raf-inhibitor complex from snapshots of the conformations obtained in 5-ns MD simulation for compound **2**: (A) when interactions with Ile463 are established and (B) when interactions with Ser465 are established.

our previous study.²⁵ Compound **2** also formed HBs with residue Ser465; compound **1** did not have HB interactions with this residue ($D_{O1-S465NH}$ in Figure 5).

Figure 9 shows the distances between the oxygen atom from the *cis*-2-hydroxycyclopentyl group of compound **3** (O_3) and residues of B-Raf forming HB with this atom during its MD simulation. Distance between the atom O_3 and the backbone carbonyl group of residue Asn580 ($D_{O3-N580}$) took values around 2.9 ± 0.2 Å at certain intervals during the MD simulation, which means that an HB between the hydroxycyclopentyl from the inhibitor and Asn580 is established. $D_{O3-N580}$ frequently took higher values and returned to take values around 2.9 Å. On the other hand, distances between O_3 and the backbone carbonyl group of residue Ser465 ($D_{O3-S465CO}$) took values close to 2.9 ± 0.2 Å when $D_{O3-N580}$ takes higher values. This indicates that compound **3** established HB interactions with the backbone of Ser465 when the HB interactions with Asn580 were broken. Time courses of $D_{O3-N580}$ and $D_{O3-S465CO}$ indicates that the O_3 does not have preference for Asn580 or Ser465, since the time of interaction with both residues is similar. We analyzed the presence of water molecules around atom O_3 , and we found that a water molecule was located between O_3 and backbone carbonyl group of residue Ser465 when O_3 had an HB interaction with Asn580 (Figure 10A). In addition, a water molecule was located between O_3 and the backbone carbonyl group of residue Asn580 when O_3 had an HB interaction with Ser465 (Figure 10B).

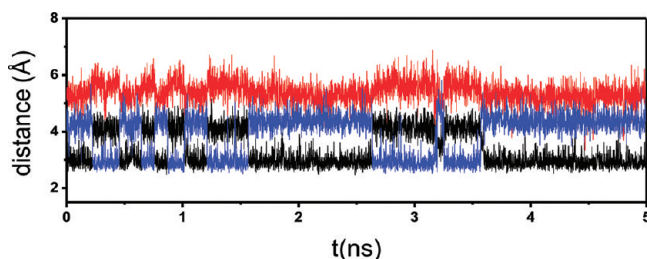


Figure 9. Distances between the oxygen atom from the *cis*-2-hydroxycyclopentyl group of compound 3 (O₃) and residues of B-Raf forming HB with this atom extracted from its 5 ns MD simulation. Distance between O₃ and the backbone carbonyl group of residue Asn580 (D_{O3-N580}) is represented in black. Distance between O₃ and the NH₂ side-chain group of Asn580 (D_{O3-N580NH2}) is represented in red. Distance between O₃ and the backbone carbonyl group of residue Ser465 (D_{O3-S465CO}) is represented in blue.

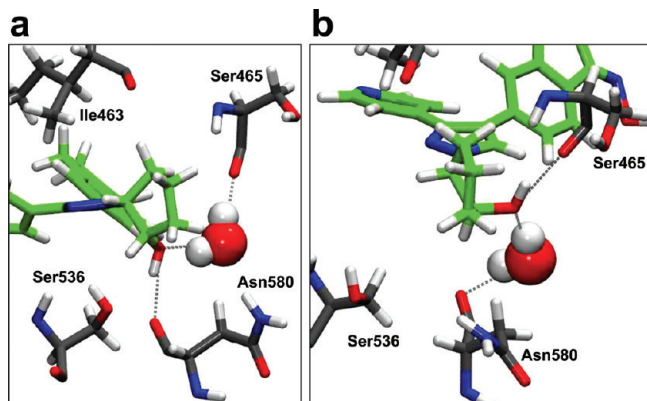


Figure 10. Hydrogen-bonding networks at the active site of the B-Raf-inhibitor complex from snapshots of the conformations obtained in 5-ns MD simulation for compound 3: (A) when interactions with Asn580 are established and (B) when interactions with Ser465 are established.

Figure 11 shows the distances between the oxygen atom from the *trans*-2-hydroxycyclopentyl group of compound 4 (O₄) and residues of B-Raf forming HB with this atom during its MD simulation. Distance between O₄ and the backbone carbonyl group of residue Asn580 (D_{O4-N580}) took values around 3.1 ± 0.4 Å the majority of time during all the 5-ns MD simulation, which means that an HB between the hydroxycyclopentyl from the inhibitor and Asn580 is established. The analysis of the distance between O₄ and the NH₂ side-chain group of Asn580 (D_{O4-N580NH2}) shows that O₄ can interact with the backbone and side chain of Asn580 at the same time (Figure 12A). On the other hand, distance between O₄ and the backbone carbonyl group of residue Ser465 (D_{O4-S465CO}) took values close to 2.8 ± 0.2 Å when D_{O4-N580} takes higher values. The time courses of D_{O4-S465CO} shows that HB interaction between atom O₄ and Ser465 (Figure 12B) is not too stable; since O₄ mainly had HB interactions with Asn580. When O₄ had HB interaction with the backbone carbonyl group of residue Asn580, and the NH₂ side-chain group of Asn580 was a little far (D_{O4-N580NH2} > 4 Å), a water molecule was located between atom O₄, NH₂ side-chain group of Asn580, and side-chain oxygen of Ser536 (Figure 12C). This water molecule was poorly refilled during the MD simulation and connected the ligand with residues Asn580 and Ser536.

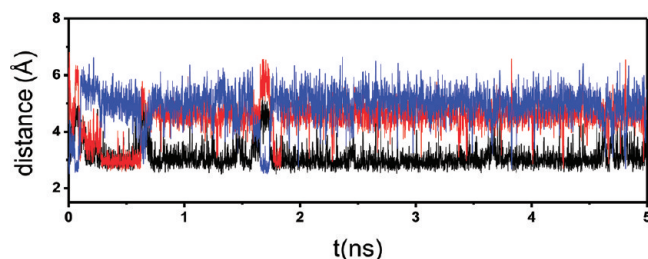


Figure 11. Distances between the oxygen atom from the *trans*-2-hydroxycyclopentyl group of compound 4 (O₄) and residues of B-Raf forming HB with this atom extracted from its 5 ns MD simulation. Distance between O₄ and the backbone carbonyl group of residue Asn580 (D_{O4-N580}) is represented in black. Distance between O₄ and the NH₂ side-chain group of Asn580 (D_{O4-N580NH2}) is represented in red. Distance between O₄ and the backbone carbonyl group of residue Ser465 (D_{O4-S465CO}) is represented in blue.

by establishing multiple HBs. The mentioned water molecule should be related with the stability of the interaction between compound 4 and the residue Asn580.

The groups at position N1 of the pyrazole ring have a different mobility since they established different HB interactions. According to MD results, the HB interactions that they have with residues in their surroundings dictate the existence of some preferred conformations. Both compounds containing 3-hydroxycyclohexyl substituents had HB interactions with the backbone carbonyl group of residue Ile463. A compound containing a hydroxyl group at position *cis* with respect to the pyrazole ring (the *R, S* diastereomer, compound 1) can establish several interactions but prefers the interaction with Ile463. However, when the hydroxyl group is at position *trans* with respect to the pyrazole ring (the *R, R* diastereomer, compound 2), HB interactions with Ile463 and Ser465 are established with similar probabilities. Compounds containing 2-hydroxycyclopentyl substituents did not establish HB interactions with Ile463; hydroxyl groups in these compounds only had HBs with the backbone of residues Asn580 and Ser465. A compound containing a hydroxyl group at position *cis* with respect to the pyrazole ring (the *R, S* diastereomer, compound 3) had HB interactions with Asn580 and Ser465. Water molecules established water bridges between the hydroxyl group and residues Asn580 or Ser465 from B-Raf, but these water molecules were constantly refilled during the MD simulation. On the other hand, compound containing a hydroxyl group at position *trans* with respect to the pyrazole ring (the *R, R* diastereomer, compound 4) prefers to interact with the backbone carbonyl group of Asn580. Dynamically stable water bridges were established between the hydroxyl group from compound 4 and residues Asn580 and Ser536; therefore, these residues could act as anchors, through the water molecule from the solvent environment, to stabilize the HB interactions with the backbone of Asn580.

As a further step to understand the biological activity trend observed for compounds 1–4, and having in mind that their potency is quite similar and depending on small structural and stereochemical changes, it is proposed and tested a new scoring function, which is derived from QM/MM calculations. It is well-known that an easy, fast, and accurate estimation of the strength of protein–ligand interactions is desired in structure based drug design, in order to rank a set of potential drugs. For instance, Hobza et al.⁵³ recently reported a PM6 based scoring function to rank a set of fifteen structurally diverse CDK2 inhibitors, which

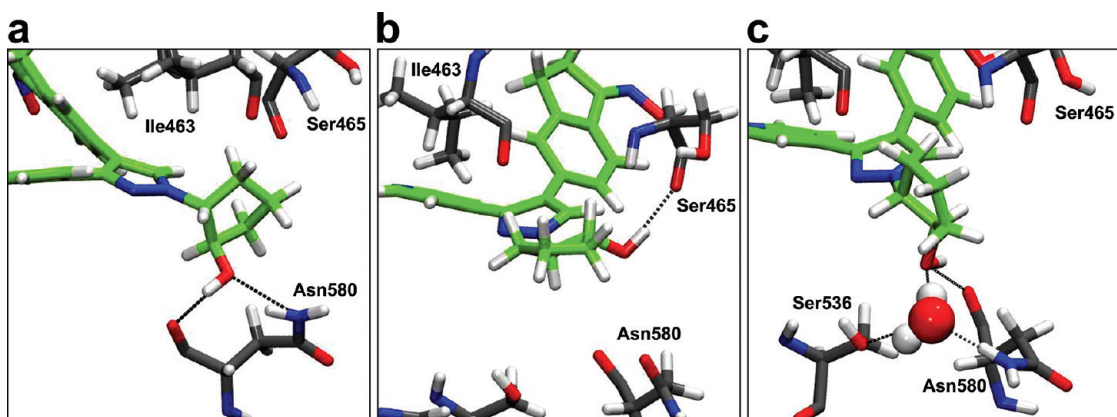


Figure 12. Hydrogen-bonding networks at the active site of the B-Raf-inhibitor complex from snapshots of the conformations obtained in 5-ns MD simulation for compound 4: (A) when interactions with side-chain and backbone of Asn580 are established at the same time, (B) when interactions with Ser465 are established, and (C) when interactions with Asn580 and Ser536 are established.

have X-ray crystal structure accessible in Protein Data Bank. They found that a new scoring function, based on an improved PM6 semiempirical method (PM6-DH2), is capable of ranking correctly all inhibitors with a statistical correlation coefficient (R^2) equal to 0.87 when compared with the experimental inhibition constants ($\ln K_i$). However, they identified the high computer time of their method as a drawback, because a single-point calculation (evaluation of one drug-receptor pose) typically took ~ 20 min (one core of Intel Core2 Quad 2.40 GHz processor) and the optimization of the CDK2–inhibitor complex took up to 3 weeks (1 core of Intel Core2 Quad 2.40 GHz processor). Here, it is presented a QM/MM derived scoring function that relies on protein–ligand structures taken from MD simulations and take advantage of the inclusion of flexibility of the complex. Besides, it avoids the need of the compound’s parametrization and proved to be less computational expensive to obtain (single point energy calculation of one drug-receptor pose takes less than 15 min in one Quad Core AMD Opteron 2.30 GHz processor) than Hobza’s based PM6 scoring function.

Previous work at our group suggested that the MD-QM/MM scoring function could be used as a predictor of biological activity and could be applied to correctly rank a small set of potent CDK2 inhibitors, and, more importantly, it was able to capture the small chemical differences between substituent groups attached to the main scaffold.^{13,21} However the MD-QM/MM calculations were very computationally expensive and not compatible with computational assisted drug design. A less demanding computational time protocol was devised, which was based on docking and the ONIOM^{54,55} approach. In that computational protocol, the initial structures were obtained from docking studies, and the ONIOM method was applied with only a single point energy calculation on the protein–ligand structure. It was obtained a good correlation model between the ONIOM derived quantum chemical descriptor “H-bond interaction energy” and the experimental biological activity, with a correlation coefficient value of $R = 0.80$ for 75 compounds.¹⁷ Nevertheless, the approach depended entirely on quality of docking poses and it lacked of consideration of protein–ligand flexibility. Also, the ONIOM method failed in the description of the dispersion interaction, and other thermodynamical terms should also have to be considered in order to improve the scoring function performance. The new QM/MM scoring function differs from previous ones in the indirect incorporation of protein–ligand flexibility

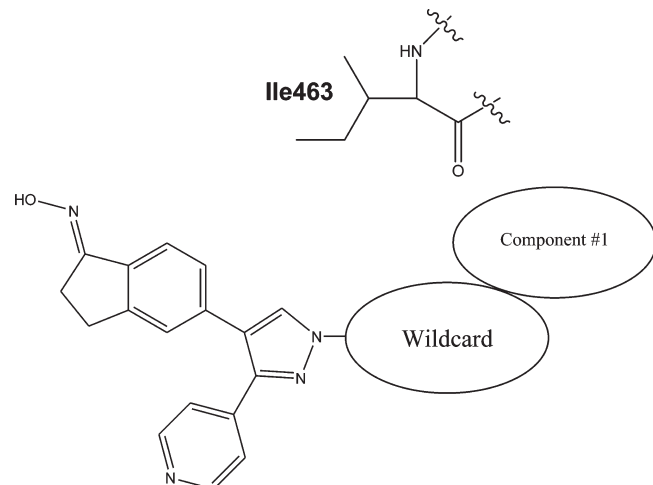


Figure 13. Chemical template for the RACHEL search.

through MD simulations, contrary to expensive MD-QM/MM simulations and static molecular docking, and the possibility to include dispersion and correlation effects with a more accurate hybrid calculation method (when compared with ONIOM approach). One factor to be considered as a possible disadvantage of our scoring function is that MM optimized structures of the ligand-protein complex usually do not represent free energy minimum for the ligand-protein complex from QM/MM calculation. However, a search for a QM minimum by using poses obtained from MD simulations can increase the computational cost, and a high computational cost prohibits the routine use of the scoring function. A possible solution to this issue should make a parameter based (for instance rmsd or distances) clusterization of several frames from MM simulations and evaluated its impact on scoring function performance.

In this work, the proposed scoring function was tested in ranking compounds 1–4, according to their biological activities measured as IC_{50} (nM) values. These compounds have small chemical and stereochemical differences and that should prove difficult and challenging to any new scoring function. As shown in Table 2, when only ligand was included in QM region and protein atoms in MM region, the QM/MM energy ($\Delta E_{QM/MM}$) obtained was capable of ranking correctly the four compounds

Table 3. Newly Designed Molecules by RACHEL Fragment-Based *De Novo* Design and Calculated Druglike Physicochemical Properties

R group (as in Figure 1)	ClogP	molecular weight (g/mol)	number of HB donors	number of HB acceptors	number of rotatable bonds	polar surface area (PSA) Å ²
RD1 (1 <i>R</i>)-3-amino-5-oxo-3-cyclohexen-1-yl	2.11	399.45	2	6	5	106.4
RD2 1-(hydroxymethyl)-4-oxo-2,5-cyclohexadien-1-yl	1.25	412.44	2	6	6	100.6
RD3 2-[(3-oxo-1-cyclopenten-1-yl)amino]ethyl	2.44	413.47	2	6	7	92.4
RD4 (1 <i>R</i>)-5-oxo-3-[(sulfanylcarbonyl)amino]-3-cyclohexen-1-yl	1.69	459.52	3	6	7	109.5
RD5 (1 <i>R</i>)-3-(formylamino)-5-oxo-3-cyclohexen-1-yl	1.57	427.46	2	6	6	109.5
RD6 (1 <i>S</i>)-3-[(2 <i>R</i>)-aziridinyl]-5-oxo-3-cyclohexen-1-yl	0.71	425.48	2	6	5	102.3
RD7 2-{[(<i>E</i>)-(2-oxodihydro-3(2 <i>H</i>)-furanylidene)methyl]amino}ethyl	2.30	429.47	2	7	7	101.6
RD8 (1 <i>R</i> ,2 <i>R</i>)-3-oxo-2-[(2 <i>R</i>)-1,3-thiazolidin-2-yl]cyclobutyl	1.73	445.54	2	6	5	92.4
RD9 1-hydroxy-4-oxo-2,5-cyclohexadien-1-yl	1.10	398.41	2	6	5	100.6
RD10 1-amino-4-oxo-2,5-cyclohexadien-1-yl	1.02	396.42	2	6	5	106.4
RD11 2-[(2-oxo-3,4-dihydro-2 <i>H</i> -pyrrol-5-yl)amino]ethyl	2.13	414.46	2	7	7	104.8
RD12 (1 <i>R</i>)-3-hydroxy-5-oxo-3-cyclohexen-1-yl	1.84	400.43	2	6	5	100.6
RD13 (1 <i>R</i> ,2 <i>S</i>)-2-[(2 <i>S</i>)-azetidinyl]-3-oxocyclobutyl	1.41	413.47	2	6	5	92.4
RD14 2-[(3,6-dioxo-1,4-cyclohexadien-1-yl)amino]ethyl	2.56	439.47	2	7	7	109.5
RD15 (1 <i>R</i>)-4-(acryloylamino)-2-oxo-3-cyclopenten-1-yl	1.50	439.47	2	6	7	109.5
RD16 2-[(3 <i>S</i>)-morpholinyl]-1-cyclopropen-1-yl	1.85	413.47	2	6	5	84.6
RD17 2-[(1 <i>H</i> -pyrrol-2-ylcarbonyl)amino]-1-cyclopropen-1-yl	3.17	436.47	3	6	7	108.2
RD18 (1 <i>R</i> ,2 <i>S</i>)-2-[(3-hydroxy-2-pyridinyl)-3-oxocyclobutyl	2.21	451.48	2	7	6	100.6
RD19 (1 <i>S</i> ,2 <i>S</i>)-2-[(2 <i>S</i>)-5-oxo-1,3-thiazolidin-2-yl]cyclopropyl	1.95	431.51	2	6	5	92.4
RD20 (1 <i>R</i> ,2 <i>S</i>)-2-[(1,6-dihydro-3-pyridinyl)-3-oxocyclobutyl	2.23	437.49	2	6	5	92.4
compounds from ref 56						
7	2.08	486.5	3	8	5	142.1
8	2.08	467.4	4	7	5	154.1
9	0.13	450.46	3	6	4	121.5
10	2.08	486.5	3	7	4	138.6

(the difference in biological activity between compounds **1** and **2** is very small and is within the range of experimental and computational measurement error), and the correlation coefficient against experimental binding free energy (ΔG_{exp}) values, derived from IC_{50} data, was 0.98. There is awareness about the significance of these previous results because it is a very small set of compounds to gain insight about the real performance of the QM/MM scoring function. In order to test more carefully the performance of proposed QM/MM scoring function, some computational experiments are actually under process, taking as targets two different protein kinase systems (CDK2 and MK2), and three bigger sets (10–15 compounds) of inhibitors with available X-ray crystallographic structure (results not published yet). Globally, it seems that new QM/MM scoring function performs well ranking the protein kinase inhibitors tested, and, more outstandingly, it is easy to obtain because no parametrization is needed for ligands and the computational cost could be dramatically reduced with the use of more powerful computer codes and hardware.

In the above MD simulations, we identified that pyrazole derivatives containing the piperidinyl group, and compounds containing *cis*- and *trans*-3-hydroxycyclohexyl groups, which are potent B-Raf inhibitors, had HB interactions with the backbone carbonyl of Ile463 at the entrance of the B-Raf active site. With this idea in mind, we carried out a RACHEL ligand-fragment based *de novo* design to obtain a data set of compounds that has this interaction as proposals of putative active candidates. The chemical template that guides the RACHEL search is represented in Figure 13. In this chemical template, Component #1

had to hydrogen bond to the backbone carbonyl of Ile463. In the wildcard region RACHEL substituted freely given the steric and electrostatic environment and added components with varying connectivity as necessary. In addition, some global descriptors were defined to consider druglikeness Lipinski⁴⁸ and Veber⁴⁹ criteria during the search. As a result, around two hundred compounds were designed. These compounds were filtered by using Ghose et al. criteria:⁵⁰ logP between −0.4 and 5.6, MW between 160 and 500 g/mol, number of atoms between 20 and 70, HB donors until 5, and HB acceptors until 10. Compounds resulting from the RACHEL design (**RD1**–**RD200**) are reported as Supporting Information. The first twenty compounds, according to RACHEL's scoring function, are reported in Table 3. In Table 3, ClogP, molecular weight, number of HB donor groups, number of HB acceptor groups, rotatable bonds, and polar surface area (PSA) values are also reported for these compounds. We verified that all compounds have favorable druglike properties according to considered criteria.^{48–50} In a recent work, Chung et al. designed some pyrazole derivatives as B-Raf inhibitors by using fragment-based *de novo* design.⁵⁶ In their search, they found four compounds that varied the R-group at the N1 position of the pyrazole ring (compounds 7–10 in ref 56). We found that these compounds have adequate ClogP, molecular weight, number of HB donor groups, number of HB acceptor groups, and rotatable bonds. However, we found that compounds 7 and 8 have PSA values of 142.1 and 154.1 Å² respectively; in this sense, they violate the Veber criterion referred to the value of PSA for having an oral bioavailability.⁴⁹

Molecules with a PSA of greater than 140 \AA^2 are usually believed to be poor at permeating cell membranes. In this sense, compounds 7 and 8 are not adequate as drugs.

CONCLUSIONS

In the current work, we proposed an efficient and simple alternative to study structure–activity relationship of ligands including i) prediction of binding modes by using flexible docking (rigid docking and MD simulations), ii) evaluation of binding energies by using conformations from MD simulations (QM/MM scoring function), and iii) proposal of new candidates by using criteria observed in MD simulations (ligand-fragment based *de novo* design).

Diastereomer N1 substituted pyrazole derivatives containing *cis*- and *trans*-3-hydroxycyclohexyl substituents (compounds **1** and **2**) and *cis*- and *trans*-2-hydroxycyclopentyl substituents (compounds **3** and **4**) have similar structures but very different activities against B-Raf kinase. The complexes between these compounds and B-Raf were studied by using bioinformatics structural methods. Docking simulations showed that all compounds had similar orientation within the B-Raf active site. MD simulations showed that all compounds established dynamically stable HB interactions with residues Glu501 and Cys532 and formed the previously described water wire connecting N2 of pyrazole ring, Cys532, and Ser536. Groups at position N1 of the pyrazole ring interacted with residues at the entrance of the active site: compound **1** mainly established HB interactions with Ile463 and occasional HB interactions with His539 and Asn580, compound **2** established HB interactions with Ile463 and Ser465, compound **3** established HB interactions with Asn580 and Ser465, and compound **4** mainly established HB interactions with Asn580 and has occasional HB interactions with Ser465.

Some inhibitor–B-Raf complex conformations obtained by MD were energetically minimized using the Embrace function within Macromodel software. Then the strength of protein–ligand complexes was evaluated based on a new quantum mechanics/molecular mechanics (QM/MM) scoring function, where the inhibitors were treated with density functional theory (DFT) methodology and the protein was modeled using OPLS-2005 force field. QM/MM single point calculations applied to twenty snapshots extracted from MD simulations, and then averaged, allowed us to correlate the potencies (calculated as binding free energies) of the studied inhibitors with QM/MM energies of the systems. Despite the small set of compounds tested in the presented work, ongoing computational experiments on additional protein kinase-ligand systems showed that the new QM/MM scoring function could prove to be useful in ranking and predicting the potency of new protein-kinase inhibitors.

Both potent inhibitors containing *cis*- and *trans*-3-hydroxycyclohexyl substituents (compounds **1** and **2**) showed interactions at the entrance of the B-Raf active site between the hydroxyl group of the inhibitors and the backbone carbonyl of residue Ile463. Previous reports, including X-ray crystallography and MD simulation, identified that this residue can also hydrogen bond to the piperidinyl group of the compound (1*E*)-5-[1-(4-piperidinyl)-3-(4-piperidinyl)-1*H*-pyrazol-4-yl]-2,3-dihydro-1*H*-inden-1-one oxime, which is also a potent inhibitor. With the proposal that the interaction with Ile463 can lead to potent B-Raf inhibitors, we designed new inhibitors by using a ligand-fragment based *de novo* design method. We obtained a data set of around two hundred compounds that have this interaction. Compounds that establish

interactions with Ile463 can be considered as proposals to have high target potency. After considering that they also have favorable druglike properties, compounds contained in our data set are proposed for synthesis and biological evaluation.

ASSOCIATED CONTENT

S Supporting Information. The newly designed molecules by fragment-based *de novo* design (Table S1). This material is available free of charge via the Internet at <http://pubs.acs.org>.

AUTHOR INFORMATION

Corresponding Author

Phone: 56-71-201 685. Fax: 56-71 201 662. E-mail: jcaballero@utalca.cl or jmcr77@yahoo.com.

ACKNOWLEDGMENT

J.C. and A.V.J. thank “Becas Universidad de Talca” for financial support from a doctoral fellowship. J.H.A.M. acknowledges the financial support from project FONDECYT No. 11100177.

REFERENCES

- (1) Sebolt-Leopold, J. S. Advances in the Development of Cancer Therapeutics Directed against the RAS-Mitogen-Activated Protein Kinase Pathway. *Clin. Cancer Res.* **2008**, *14*, 3651–3656.
- (2) Mercer, K. E.; Pritchard, C. A. Raf proteins and cancer: B-Raf is identified as a mutational target. *Biochim. Biophys. Acta* **2003**, *1653*, 25–40.
- (3) Garnett, M. J.; Marais, R. Guilty as charged: B-RAF is a human oncogene. *Cancer Cell* **2004**, *6*, 313–319.
- (4) Safety Study of PLX4032 in Patients With Solid Tumors. Clinical Trials; National Institutes of Health: Bethesda, MD, *ClinicalTrials.gov*; Identifier: NCT00405587.
- (5) Study of XL281 in Adults With Solid Tumors. Clinical Trials; National Institutes of Health: Bethesda, MD, *ClinicalTrials.gov*; Identifier: NCT00451880.
- (6) A Phase I Study to Investigate the Safety, Pharmacokinetics, and Pharmacodynamics of GSK2118436 in Subjects With Solid Tumors. Clinical Trials; National Institutes of Health: Bethesda, MD, *ClinicalTrials.gov*; Identifier: NCT00880321.
- (7) Ramnath, N.; Adjei, A. Inhibitors of Raf kinase and MEK signaling. *Update Cancer Ther.* **2007**, *2*, 111–118.
- (8) Fernandez, M.; Tundidor-Camba, A.; Caballero, J. Modeling of Cyclin-Dependent Kinase Inhibition by 1*H*-Pyrazolo[3,4-d]Pyrimidine Derivatives Using Artificial Neural Network Ensembles. *J. Chem. Inf. Model.* **2005**, *45*, 1884–1895.
- (9) González, M.; Caballero, J.; Helguera, A.; Garriga, M.; González, G.; Fernández, M. 2D Autocorrelation Modelling of the Inhibitory Activity of Cytokinin-Derived Cyclin-Dependent Kinase Inhibitors. *Bull. Math. Biol.* **2006**, *68*, 735–751.
- (10) Caballero, J.; Fernández, M.; Saavedra, M.; González-Nilo, F. D. 2D Autocorrelation, CoMFA, and CoMSIA modeling of protein tyrosine kinases’ inhibition by substituted pyrido[2,3-d]pyrimidine derivatives. *Bioorg. Med. Chem.* **2008**, *16*, 810–821.
- (11) Caballero, J.; Fernández, M.; González-Nilo, F. D. Structural requirements of pyrido[2,3-d]pyrimidin-7-one as CDK4/D inhibitors: 2D autocorrelation, CoMFA and CoMSIA analyses. *Bioorg. Med. Chem.* **2008**, *16*, 6103–6115.
- (12) Gueto, C.; Ruiz, J. L.; Torres, J. E.; Méndez, J.; Vivas-Reyes, R. Three-dimensional quantitative structure-activity relationship studies on novel series of benzotriazine based compounds acting as Src

- inhibitors using CoMFA and CoMSIA. *Bioorg. Med. Chem.* **2008**, *16*, 2439–2447.
- (13) Alzate-Morales, J.; Caballero, J. Computational Study of the Interactions between Guanine Derivatives and Cyclin-Dependent Kinase 2 (CDK2) by CoMFA and QM/MM. *J. Chem. Inf. Model.* **2010**, *50*, 110–122.
- (14) Caballero, J.; Quiliano, M.; Alzate-Morales, J. H.; Zimic, M.; Deharo, E. Docking and quantitative structure–activity relationship studies for 3-fluoro-4-(pyrrolo[2,1-f][1,2,4]triazin-4-yloxy)aniline, 3-fluoro-4-(1H-pyrrolo[2,3-b]pyridin-4-yloxy)aniline, and 4-(4-amino-2-fluorophenoxy)-2-pyridinylamine derivatives as c-Met kinase inhibitors. *J. Comput.-Aided Mol. Des.* **2011**, *25*, 349–369.
- (15) Muthas, D.; Sabnis, Y. A.; Lundborg, M.; Karlén, A. Is it possible to increase hit rates in structure-based virtual screening by pharmacophore filtering? An investigation of the advantages and pitfalls of post-filtering. *J. Mol. Graphics Modell.* **2008**, *26*, 1237–1251.
- (16) Xie, H.-Z.; Li, L.-L.; Ren, J.-X.; Zou, J.; Yang, L.; Wei, Y.-Q.; Yang, S.-Y. Pharmacophore modeling study based on known spleen tyrosine kinase inhibitors together with virtual screening for identifying novel inhibitors. *Bioorg. Med. Chem. Lett.* **2009**, *19*, 1944–1949.
- (17) Alzate-Morales, J. H.; Caballero, J.; Vergara-Jaque, A.; González-Nilo, F. D. Insights into the structural basis of N2 and O6 substituted guanine derivatives as cyclin-dependent kinase 2 (CDK2) inhibitors: prediction of the binding modes and potency of the inhibitors by docking and ONIOM calculations. *J. Chem. Inf. Model.* **2009**, *49*, 886–899.
- (18) Larsen, C. A.; Bisson, W. H.; Dashwood, R. H. Tea Catechins Inhibit Hepatocyte Growth Factor Receptor (MET Kinase) Activity in Human Colon Cancer Cells: Kinetic and Molecular Docking Studies. *J. Med. Chem.* **2009**, *S2*, 6543–6545.
- (19) Uno, M.; Ban, H. S.; Nabeyama, W.; Nakamura, H. de novo Design and synthesis of N-benzylanilines as new candidates for VEGFR tyrosine kinase inhibitors. *Org. Biomol. Chem.* **2008**, *6*, 979–981.
- (20) Vieth, M.; Erickson, J.; Wang, J.; Webster, Y.; Mader, M.; Higgs, R.; Watson, I. Kinase Inhibitor Data Modeling and de Novo Inhibitor Design with Fragment Approaches. *J. Med. Chem.* **2009**, *52*, 6456–6466.
- (21) Alzate-Morales, J. H.; Contreras, R.; Soriano, A.; Tuñon, I.; Silla, E. A Computational Study of the Protein-Ligand Interactions in CDK2 Inhibitors: Using Quantum Mechanics/Molecular Mechanics Interaction Energy as a Predictor of the Biological Activity. *Biophys. J.* **2007**, *92*, 430–439.
- (22) Gleeson, M. P.; Gleeson, D. QM/MM As a Tool in Fragment Based Drug Discovery. A Cross-Docking, Rescoring Study of Kinase Inhibitors. *J. Chem. Inf. Model.* **2009**, *49*, 1437–1448.
- (23) Alzate-Morales, J. H.; Caballero, J.; Gonzalez-Nilo, F. D.; Contreras, R. A computational ONIOM model for the description of the H-bond interactions between NU2058 analogues and CDK2 active site. *Chem. Phys. Lett.* **2009**, *479*, 149–155.
- (24) Villacañas, O.; Pérez, J. J.; Rubio-Martínez, J. Structural Analysis of the Inhibition of Cdk4 and Cdk6 by p16INK4a Through Molecular Dynamics Simulations. *J. Biomol. Struct. Dynamics* **2002**, *20*, 347–358.
- (25) Alzate-Morales, J. H.; Vergara-Jaque, A.; Caballero, J. Computational Study on the Interaction of N1 Substituted Pyrazole Derivatives with B-Raf Kinase: An Unusual Water Wire Hydrogen-Bond Network and Novel Interactions at the Entrance of the Active Site. *J. Chem. Inf. Model.* **2010**, *50*, 1101–1112.
- (26) Luo, C.; Xie, P.; Marmorstein, R. Identification of BRAF Inhibitors through In Silico Screening. *J. Med. Chem.* **2008**, *S1*, 6121–6127.
- (27) Fratev, F.; Jónsdóttir, S. An in silico study of the molecular basis of B-RAF activation and conformational stability. *BMC Struct. Biol.* **2009**, *9*, 47.
- (28) Fratev, F.; Jónsdóttir, S. Ó.; Mihaylova, E.; Pajeva, I. Molecular Basis of Inactive B-RAFWT and B-RAFV600E Ligand Inhibition, Selectivity and Conformational Stability: An in Silico Study. *Mol. Pharmaceutics* **2009**, *6*, 144–157.
- (29) Moretti, S.; De Falco, V.; Tamburrino, A.; Barbi, F.; Tavano, M.; Avenia, N.; Santeusanio, F.; Santoro, M.; Macchiarulo, A.; Puxeddu, E. Insights into the molecular function of the inactivating mutations of B-Raf involving the DFG motif. *Biochim. Biophys. Acta, Mol. Cell Res.* **2009**, *1793*, 1634–1645.
- (30) Hansen, J. D.; Grina, J.; Newhouse, B.; Welch, M.; Topalov, G.; Littman, N.; Callejo, M.; Gloor, S.; Martinson, M.; Laird, E.; Brandhuber, B. J.; Vigers, G.; Morales, T.; Woessner, R.; Randolph, N.; Lyssikatos, J.; Olivero, A. Potent and selective pyrazole-based inhibitors of B-Raf kinase. *Bioorg. Med. Chem. Lett.* **2008**, *18*, 4692–4695.
- (31) Zaheer-ul-haq; Wellenzohn, B.; Liedl, K. R.; Rode, B. M. Molecular Docking Studies of Natural Cholinesterase-Inhibiting Steroidal Alkaloids from Sarcococca saligna. *J. Med. Chem.* **2003**, *46*, 5087–5090.
- (32) Rojo, L. E.; Alzate-Morales, J.; Saavedra, I. N.; Davies, P.; MacCioni, R. B. Selective Interaction of Lansoprazole and Astemizole with Tau Polymers: Potential New Clinical Use in Diagnosis of Alzheimer's Disease. *J. Alzheimer Dis.* **2010**, *19*, 573–589.
- (33) Hanessian, S.; Moitessier, N.; Therrien, E. A comparative docking study and the design of potentially selective MMP inhibitors. *J. Comput.-Aided Mol. Des.* **2001**, *15*, 873–881.
- (34) Caballero, J.; Vergara-Jaque, A.; Fernández, M.; Coll, D. Docking and quantitative structure–activity relationship studies for sulfonyl hydrazides as inhibitors of cytosolic human branched-chain amino acid aminotransferase. *Mol. Diversity* **2009**, *13*, 493–500.
- (35) Lagos, C. F.; Caballero, J.; Gonzalez-Nilo, F. D.; David Pessoa-Mahana, C.; Perez-Acle, T. Docking and quantitative structure-activity relationship studies for the bisphenylbenzimidazole family of non-nucleoside inhibitors of HIV-1 reverse transcriptase. *Chem. Biol. Drug Des.* **2008**, *72*, 360–369.
- (36) Abagyan, R.; Totrov, M.; Kuznetsov, D. ICM - A new method for protein modeling and design: Applications to docking and structure prediction from the distorted native conformation. *J. Comput. Chem.* **1994**, *15*, 488–506.
- (37) *Molecular Ed., version 2.5*; Molsoft LLC: La Jolla, CA, 2006.
- (38) *ICM, version 3.4–8*; Molsoft LLC: La Jolla, CA, 2006.
- (39) An, J.; Totrov, M.; Abagyan, R. Pocketome via Comprehensive Identification and Classification of Ligand Binding Envelopes. *Mol. Cell. Proteomics* **2005**, *4*, 752–761.
- (40) Kaminski, G. A.; Friesner, R. A.; Tirado-Rives, J.; Jorgensen, W. L. Evaluation and Reparametrization of the OPLS-AA Force Field for Proteins via Comparison with Accurate Quantum Chemical Calculations on Peptides. *J. Phys. Chem. B* **2001**, *105*, 6474–6487.
- (41) *Desmond Molecular Dynamics System, version 2.2*, 2009; D. E. Shaw Research, Schrödinger, LLC: New York, NY.
- (42) Bowers, K. J.; Chow, E.; Xu, H.; Dror, R. O.; Eastwood, M. P.; Gregersen, B. A.; Klepeis, J. L.; Kolossvary, I.; Moraes, M. A.; Sacerdoti, F. D.; Salmon, J. K.; Shan, Y.; Shaw, D. E. In *Proceedings of the 2006 ACM/IEEE conference on Supercomputing*; ACM: Tampa, FL, 2006; p 84.
- (43) *MacroModel, version 9.5*, 2007; Schrödinger, LLC: New York, NY.
- (44) Humphrey, W.; Dalke, A.; Schulter, K. VMD: Visual molecular dynamics. *J. Mol. Graph.* **1996**, *14*, 33–38.
- (45) *QSite, version 5.5*, 2009; Schrödinger, LLC: New York, NY.
- (46) Ho, C. M. W. In *Chemoinformatics in Drug Discovery*; Oprea, T. I., Ed.; Wiley-VCH Verlag: 2005; pp 199–219.
- (47) Head, R. D.; Smythe, M. L.; Oprea, T. I.; Waller, C. L.; Green, S. M.; Marshall, G. R. VALIDATE: A New Method for the Receptor-Based Prediction of Binding Affinities of Novel Ligands. *J. Am. Chem. Soc.* **1996**, *118*, 3959–3969.
- (48) Lipinski, C. A.; Lombardo, F.; Dominy, B. W.; Feeney, P. J. Experimental and computational approaches to estimate solubility and permeability in drug discovery and development settings. *Adv. Drug Delivery Rev.* **1997**, *23*, 3–25.
- (49) Veber, D. F.; Johnson, S. R.; Cheng, H.-Y.; Smith, B. R.; Ward, K. W.; Kopple, K. D. Molecular Properties That Influence the Oral Bioavailability of Drug Candidates. *J. Med. Chem.* **2002**, *45*, 2615–2623.
- (50) Ghose, A. K.; Viswanadhan, V. N.; Wendoloski, J. J. A Knowledge-Based Approach in Designing Combinatorial or Medicinal Chemistry Libraries for Drug Discovery. 1. A Qualitative and Quantitative

Characterization of Known Drug Databases. *J. Comb. Chem.* **1999**, *1*, 55–68.

(S1) Wang, X.; Berger, D. M.; Salaski, E. J.; Torres, N.; Hu, Y.; Levin, J. I.; Powell, D.; Wojciechowicz, D.; Collins, K.; Frommer, E. Discovery of highly potent and selective type I B-Raf kinase inhibitors. *Bioorg. Med. Chem. Lett.* **2009**, *19*, 6571–6574.

(S2) King, A. J.; Patrick, D. R.; Batorsky, R. S.; Ho, M. L.; Do, H. T.; Zhang, S. Y.; Kumar, R.; Rusnak, D. W.; Takle, A. K.; Wilson, D. M.; Hugger, E.; Wang, L.; Karreth, F.; Lougheed, J. C.; Lee, J.; Chau, D.; Stout, T. J.; May, E. W.; Rominger, C. M.; Schaber, M. D.; Luo, L.; Lakdawala, A. S.; Adams, J. L.; Contractor, R. G.; Smalley, K. S. M.; Herlyn, M.; Morrissey, M. M.; Tuveson, D. A.; Huang, P. S. Demonstration of a Genetic Therapeutic Index for Tumors Expressing Oncogenic BRAF by the Kinase Inhibitor SB-590885. *Cancer Res.* **2006**, *66*, 11100–11105.

(S3) Dobeš, P.; Fanfrlík, J.; Řezáč, J.; Otyepka, M.; Hobza, P. Transferable scoring function based on semiempirical quantum mechanical PM6-DH2 method: CDK2 with 15 structurally diverse inhibitors. *J. Comput.-Aided Mol. Des.* **2011**, *25*, 223–235.

(S4) Svensson, M.; Humbel, S.; Froese, R. D. J.; Matsubara, T.; Sieber, S.; Morokuma, K. ONIOM: A Multilayered Integrated MO + MM Method for Geometry Optimizations and Single Point Energy Predictions. A Test for Diels–Alder Reactions and Pt(P(t-Bu)₃)₂ + H₂ Oxidative Addition. *J. Phys. Chem.* **1996**, *100*, 19357–19363.

(S5) Dapprich, S.; Komáromi, I.; Byun, K. S.; Morokuma, K.; Frisch, M. J. A new ONIOM implementation in Gaussian98. Part I. The calculation of energies, gradients, vibrational frequencies and electric field derivatives. *J. Mol. Struct. THEOCHEM* **1999**, *461*–462, 1–21.

(S6) Chung, J. Y.; Chung, H. W.; Cho, S. J.; Hah, J.-M.; Cho, A. E. QM/MM based 3D QSAR models for potent B-Raf inhibitors. *J. Comput.-Aided Mol. Des.* **2010**, *24*, 385–397.